First insight in element localisation in different body parts of the acanthocephalan Dentitruncus truttae using TEM and NanoSIMS

Vlatka Filipović Marijić, Maria Angels Subirana, Dirk Schaumlöffel, Josip Barišić, Étienne Gontier, Nesrete Krasnići, Tatjana Mijošek, Jesús Hernández-Orts, Tomáš Scholz, Marijana Erk

First insight in element localisation in different body parts of the acanthocephalan *Dentitruncus truttae* using TEM and NanoSIMS

Vlatka Filipović Marijić[*, 1], *Maria Angels Subirana*[2], *Dirk Schaumlöffel*[2], *Josip Barišić*[3], *Etienne Gontier*[4], *Nesrete Krasnići*[1, †], *Tatjana Mijošek*[1], *Jesús S. Hernández-Orts*[5, 6], *Tomáš Scholz*[5], *Marijana Erk*[1, #]

[1]Ruđer Bošković Institute, Division for Marine and Environmental Research, Laboratory for Biological Effects of Metals, Bijenička c. 54, 10000 Zagreb, Croatia

[2]CNRS, Université de Pau et des Pays de l'Adour, E2S UPPA, Institut des Sciences Analytiques et de Physico-Chimie pour l'Environnement et les Matériaux (IPREM), UMR 5254, 64000 Pau, France

[3]WellFish Diagnostics, Paisley, Scotland, UK

[4]Université Bordeaux, CNRS, INSERM, Bordeaux Imaging Center, BIC, UAR 3420, US 4, F-33000 Bordeaux, France

[5]Institute of Parasitology, Biology Centre, Czech Academy of Sciences, Branišovská 31, 370 05, České Budějovice, Czech Republic

[6]Natural History Museum, London, Cromwell Road, London, SW7 5BD, United Kingdom

***Corresponding author:**

Vlatka Filipović Marijić

Laboratory for Biological Effects of Metals

Division for Marine and Environmental Research

Ruđer Bošković Institute

Bijenička c. 54, 10000 Zagreb, Croatia

e-mail: vfilip@irb.hr

Present Addresses

[†] University of Vienna, Department of Structural and Computational Biology, 25 Campus-Vienna-Biocenter 5, 1030 Vienna, Austria

[#] Ruđer Bošković Institute, Division of Molecular Medicine, Laboratory for Bioanalytics, Bijenička c. 54, 10000 Zagreb, Croatia

Abstract

Acanthocephalans, intestinal parasites of vertebrates, are characterised by orders of magnitude higher metal accumulation than free-living organisms, but the mechanism of such effective metal accumulation is still unknown. The aim of our study was to gain a new knowledge on high-resolution element localisation in acanthocephalans' body as an initial step in revealing metal uptake and accumulation in organisms in real environmental conditions. For the first time, nanoscale secondary ion mass spectrometry (NanoSIMS) was applied for high-resolution mapping of 12 elements (C, Ca, Cu, Fe, N, Na, O, P, Pb, S, Se, and Tl) in the ultrastructure of three selected body parts (trunk spines, inner part of the proboscis receptacle and inner surface of the tegument) in *Dentitruncus truttae*, hosted in the brown trout (*Salmo trutta*) from the Krka River in Croatia. In addition, the same body parts were analysed by transmission electron microscopy (TEM) and correlated to NanoSIMS images. . Metal concentrations, determined by HR ICP-MS, confirmed higher accumulation in *D. truttae* than in the fish intestine. The chemical composition of the acanthocephalan body showed the highest density in all studied structures for C, Ca, N, Na, O, S, as important and constitutive elements in living cells, while Fe was predominant among trace elements. Generally, higher element density was recorded in trunk spines and tegument, as body structures responsible for substance absorbance in parasites. The results obtained by NanoSIMS and TEM-NanoSIMS correlative imaging represent pilot data on element mapping with nanoscale resolution in the ultrastructure of different body parts of acanthocephalans and generally, give contribution for the further application of this technique in any parasite species.

Keywords: nanoscale secondary ion mass spectrometry, transmission electron microscopy, correlative imaging, thorny-headed worms, body ultrastructure, chemical composition

1. INTRODUCTION

Nanoscale secondary ion mass spectrometry (NanoSIMS), as a type of imaging mass spectrometry, represents a technique for elemental imaging of high sensitivity, high spatial and mass resolution, and a powerful tool in tracking molecules and quantifying biological processes at subcellular level (Guerquin-Kern et al., 2005). Although, NanoSIMS contributed significantly in the last two decades to the fieldof biology, especially to microbiology (Kleinfeld et al., 2004), it has not previously been applied for high-resolution multi-element mapping in the ultrastructure of any parasite species. Such data can represent an important contribution for future application in environmental studies. As parasitism is among most common lifestyles on the earth, there is certainly a need for investigating parasites and their role in aquatic ecosystems, as well as their impact on the environmental health. Investigation of parasites by NanoSIMS serves as a base for future application in environmental parasitology and metal accumulation in biota. Further, as acanthocephalans are already known as effective metal accumulators, they are successfully applied as indicators of water quality in biomonitoring studies (Sures, 2004; Thielen et al., 2004; Filipović Marijić et al., 2013, 2014, 2022) and a novel field, Environmental Parasitology, was established regarding the linkage between contamination and parasitism (Sures et al., 2017). Although present in fish intestines, acanthocephalans were confirmed as relevant bioindicators of environmental conditions, reflecting metal exposure in accordance to fish soft and hard tissues (Filipović Marijić et al., 2022). With respect to morphology, the ultrastructure of acanthocephalans has been studied by scanning electron microscopy (SEM) (Taraschewski, 2000). However, the localization of chemical elements in their structure is limited so far to few studies using energy dispersive X-ray analysis for the detection of major elements in

micrometer-sized spots, mainly in the hooks of the proboscis of the parasite (Heckmann et al., 2007, 2012a, b). Therefore, our aim was to acquire the first data on high-resolution element and metal localisation in the ultrastructure of acanthocephalans' body, which may help to understand the mechanisms of metal uptake in environmental conditions.

Acanthocephalans is a small group of endoparasites, included in the taxon Syndermata (Mauer et al., 2021). They use Mandibulata (Arthropoda) as intermediate hosts and jawed vertebrates (Gnathostomata), often teleost fish, as definitive hosts (Kennedy, 2006). Although endoparasites are not directly exposed to the environment, they are highly affected, indirectly via their hosts and numerous studies have demonstrated utility of fish parasites to detect changes in polluted environments (Thielen et al., 2004; Nachev et al., 2013; Sures, 2014; Filipović Marijić et al., 2022). In addition, acanthocephalans were also shown to have a possible protective role against metal accumulation in their hosts (Oyoo-Okoth et al., 2012, Filipović Marijić et al., 2013, 2014). Accordingly, it is important to investigate complex parasite-host relationship and metal uptake, especially in environmental conditions where parasites can significantly affect responses of their hosts, but are often neglected in research.

In the absence of data on metal accumulation or high-resolution elemental mapping in different body parts of acanthocephalans, our data may provide a step forward in understanding the successful metal uptake and storage and in observing which body parts are responsible for effective metal absorption. For that purposes, the acanthocephalan *Dentitruncus truttae* Sinzar, 1955, a parasite of brown trout (*Salmo trutta* L.), which is native in the karst Krka River in Croatia, was studied. Hence, the specific objective of the present study was to examine and compare the ultrastructure and localisation of 12 elements (C, Ca, Cu, Fe, N, Na, O, P, Pb, S, Se and Tl) at nanometer level in three representative acanthocephalan body parts (trunk spines,

proboscis receptacle and inner surface of the tegument) using transmission electron microscopy (TEM) and NanoSIMS analyses, as well as the correlation of both imaging techniques. Non-metals were selected as essential elements in all living organisms (C, N, O, P, S), while metal(loid)s were chosen as essential macroelements (Ca, Na) and trace elements (Fe, Cu, Se), and moreover non-essential metals (Pb, Tl), showing different roles and concentrations in the organisms. As previously stated by Taraschewski (2000) and Heckmann et al. (2012a), knowledge of the structure and chemical composition of acanthocephalans may help us to understand effective mechanisms of uptake and storage of chemical substances, and to clarify their roles and utilisation in the biology of these parasites.

2. MATERIALS AND METHODS

2.1 Study area and sampling procedure

Samples of trout and their acanthocephalan parasites were taken from the Krka River, a typical karstic river flowing through the Dinaric carbonate area of the Republic of Croatia. Detailed map of the sampling area and physico-chemical water characteristics were provided by Filipović Marijić et al. (2018) and Sertić Perić et al. (2018). Brown trout were sampled in the river source to estimate physiological conditions without pollution disturbances and in May 2016 to avoid physiology-related metal variability during fish spawning period, which occurs in late autumn. At the same time, water was sampled for metal analyses, pointing to increasing trend in metal concentrations downstream due to contamination from industrial (Fe, Se, Pb) and municipal (Cu) effluents, except for comparable or higher Tl levels at the river source (Dragun et

al., 2018, Filipović Marijić et al., 2018). Sampling was performed by electrofishing, in accordance with the Croatian standard legislation of fish sampling by electric power (HRN EN 14011, 2005). In total, 13 fish individuals were sampled and all of them were infected with acanthocephalans, containing 269 acanthocephalans and resulting with a mean intensity of infection 20.7 ± 8.9. Detailed data on fish biometry and acanthocephalan epidemiological characteristics can be found in Mijošek et al. (2022). Captured fish were kept alive in aerated water until further processing in the laboratory.

After trouts were anesthetized with tricaine methanesulfonate (MS 222 Sigma Aldrich) in accordance with the Ordinance on the Protection of Animals used for scientific purposes (NN 55/2013) and sacrificed, the gastrointestinal tract (stomach, pyloric caeca and the anterior, middle and posterior portions of the intestine) was removed and opened along its entire length and carefully checked for the presence of intestinal parasites. Acanthocephalans found were gently detached from the intestine using tweezers, counted per each specimen and isolated for the further NanoSIMS and metal analyses. Collected acanthocephalans were identified as *Dentitruncus truttae* following Manilla et al. (1976), Dezfuli et al. (2008b) and Vardić Smrzlić et al. (2013) This species represents the only member of the genus *Dentitruncus* Sinzar, 1955 of the family Illiosentidae Golvan, 1960 and occurs only in the limited areas of Bosnia and Herzegovina (Šinžar, 1955), Italy (Dezfuli et al., 2008b) and Croatia (Topić Popović et al.,1999; Vardić Smrzlić et al., 2013). It was reported that *D. truttae* can cause serious intestinal damage to its fish host (Dezfuli et al., 2008a) and, similar to other acanthocephalans, it can effectively accumulate metals and be considered as an indicator of metal exposure in the aquatic environment (Filipović Marijić et al., 2022; Mijošek et al., 2022).

Specimens used for TEM and NanoSIMS analyses were initially chemically fixed by the procedure explained in section 2.3. To compare metal localisation in different body parts of the parasite, all analyses were performed in the same parasite individual of *D. truttae*. Other acanthocephalan individuals (n = 10) isolated from the same host as those used for NanoSIMS analyses were immediately stored at -80 °C for metal analyses. In addition, the posterior intestine of the host fish (total length 22.1 cm, total body mass 107.2 g) was dissected, carefully removing gut content and parasites, then washed with phosphate buffered saline and stored at -80°C for further metal analysis.

2.2 Determination of total metal concentrations in acanthocephalans and fish intestine

Prior to the metal measurements, the wet tissue of the posterior part of intestine (0.06 g) of the brown trout hosting acanthocephalan intended for NanoSIMS analyses and whole acanthocephalans (composite sample of 0.02 g) were digested using the oxidation mixture of concentrated HNO_3 (Rotipuran® Supra 69%, Carl Roth, Germany) and 30% H_2O_2 (Suprapur®, Merck, Germany) in the volume ratio of 3 : 1. The digestions were performed at 85 ºC for 3.5 h in the dry oven. Metal concentrations were determined in the appropriately diluted samples using high resolution inductively coupled plasma mass spectrometer (HR ICP-MS, Element 2; Thermo Finnigan, Bremen, Germany), equipped with an autosampler SC-2 DX FAST (Elemental Scientific, USA). Measurements of ^{208}Pb, ^{80}Se and ^{205}Tl were performed in low-resolution mode and of ^{23}Na, ^{42}Ca, ^{56}Fe, ^{63}Cu in medium-resolution mode. Indium (In, 1 μg L^{-1}, Atomic Spectroscopy Standard Solution, Fluka, Seelze, Germany) was added, prior to the measurements, to all solutions as an internal standard.

Two external calibrations were performed, one for trace elements using multielement stock standard solution (Analytika, Prague, Czech Republic) and the other for the macroelements using standard containing Na (1.0 g L^{-1}) and Ca (2.0 g L^{-1}) (Fluka, Seelze, Germany Germany). The accuracy and precision of metal determination by HR ICP-MS was controlled by the analysis of the certified reference material DORM-2 (National Research Council, Canada), previously digested in the same way as parasites and fish intestine. Agreement between performed measurements and certified values was generally good, resulting in the following recovery values (%, mean ± S.D.): Cu 100±3.1, Fe 101±5.0, Se 102±5.1, Tl 101±12.3, Pb 118.5±15.2. The ratio of metal levels in parasites to that in the fish intestine was calculated and considered as bioconcentration factor (BCF) according to Sures et al. (1999), in order to be consistent with other studies dealing with similar topics.

2.3 Sample preparation for TEM and NanoSIMS analyses

Samples were fixed in two steps due to the long geographic distance between the sampling site in Croatia and the sample preparation laboratory at the Bordeaux Imaging Centre (BIC) in France. Pre-fixation of acanthocephalan tissue was performed at the nearby veterinary ambulance in the town of Knin, close to the Krka River sampling site, using 2 % paraformaldehyde and 2.5 % glutaraldehyde in 0.1 M of phosphate buffer according to a standard procedure (Hayat, 1982; Graham and Orenstein, 2007). After 4 hours at room temperature, samples were cooled down to 4 °C (Graham and Orenstein, 2007). The mixture of paraformaldehyde and glutaraldehyde was employed at room temperature allowed thus rapid and efficient fixation. Then, the pre-fixed tissue samples were shipped by express mail to BIC.

Acanthocephalans stored in buffer solution were refrigerated during shipping and the sample pre-fixation process took less than 2 days.

At BIC, samples were rinsed with 0.1 M phosphate buffer and post-fixed with 1% osmium tetroxide in 0.1 M phosphate buffer for 2 h. Afterwards, they were dehydrated by a stepwise gradient of ethanol (50, 70, 90, 100 %, at 37 °C for 19 min) and impregnated with epoxy resin (EPON 812, Delta Microscopies, Mauressac, France) with a graded series of ethanol : resin mixtures with increasing resin fraction (3 : 1, 1 : 1, 1 : 3, pure resin, at 40–50 °C for a total of 55 min) using an automatic microwave tissue processor Leica EM AMW (Leica Microsystems, Vienna, Austria). Finally, the resin was polymerized at 83 °C for 105 min.(Schroeder et al., 2006).

The resin blocs were cut with an ultramicrotome (EM Ultracut-UC7, Leica Microsystems, Vienna, Austria) using a diamond knife (Diatome, Biel-Bienne, Switzerland). For TEM-NanoSIMS correlative imaging, subsequent sections of 70 nm thickness for TEM and of 300 nm for NanoSIMS were cut. The TEM sections were placed on copper grids and NanoSIMS sections were placed on silicon wafers (Ted Pella, Redding, USA). Samples for NanoSIMS analyses were shipped from the BIC to the Institut des Sciences Analytiques et de Physico-Chimie pour l'Environnement et les Matériaux (IPREM), Université de Pau et des Pays de l'Adour, France.

2.4 TEM analysis

Localisation of the subcellular structures and definition of regions of interest of *D. truttae* at nanometer (nm) level was performed by TEM (Hitachi H7650, Tokyo, Japan; ×3000 to

×20000). This allowed imaging of subcellular structures (three regions of the anterior metasoma, i.e., trunk spine, proboscis receptacle and the inner surface of the tegument) and superposing them to NanoSIMS images. In this way, subcellular structures recorded by TEM were explained in detail in the acanthocephalan body and were correlated to elemental images obtained by NanoSIMS. Terminology of subcellular structures follows Beermann et al. (1974), Dezfuli and Sbrenna (1990), Taraschewski (2000), Herlyn and Ehlers (2001) and Herlyn and Taraschewski (2017).

2.5 NanoSIMS analysis

High resolution secondary ion mass spectrometry analysis with a NanoSIMS 50L (Cameca, Gennevilliers, France) was used to examine the elemental distribution in the acanthocephalan tissues. The recent implementation of a bright radio frequency plasma O^- primary ion source in NanoSIMS for the generation of positive secondary ions allows the mapping of major and trace metals in tissue and cells with a spatial resolution down to 40 nm (Malherbe et al., 2016). In our study, the Hyperion^{TM} RF plasma primary oxygen ion source was used for the mapping of the electropositive elements: sodium ($^{23}Na^+$), calcium ($^{40}Ca^+$), iron ($^{56}Fe^+$), copper ($^{63}Cu^+$), thallium ($^{205}Tl^+$), lead ($^{208}Pb^+$), and carbon ($^{12}C^+$) [6]. Subsequently, a primary Cs^+ ion source was used for the mapping in the same spots of electronegative elements: carbon ($^{12}C_2^-$), nitrogen ($^{12}C^{14}N^-$), oxygen ($^{16}O^-$), sulphur ($^{32}S^-$), selenium ($^{80}Se^-$) and phosphorus ($^{31}P^{16}O_2^-$), with the cluster atoms selected to achieve higher signal intensity. The elements were measured in multicollection mode with seven parallel electron multiplier detectors and the mass

247 resolution was adjusted to resolve possible interferences. For both ion sources, the carbon signal
248 was used for data normalization.
249 Regions of interest in the tissue were selected using an integrated Charged Coupled
250 Device (CCD) camera, and then analyzed by NanoSIMS with a raster size of 55 × 55 µm, with
251 256 × 256 pixels, with a dwell time of 10 ms per pixel. A beam of 8.5 pA was applied on the
252 sample with the oxygen ion source, and of 1.0 pA with the cesium ion source, after a pre-
253 sputtering of the sample surface during 10 min at about 100 pA. Image processing was
254 performed using WinImage (Cameca). A total of 50 cycles of the same area were acquired and
255 they were stacked to obtain the final image. Normalization over the carbon signal was also
256 performed, as well as overlays of several elements for better visualization of data.
257
258 **3. RESULTS AND DISCUSSION**
259
260 **3.1 Metal concentrations in acanthocephalans and trout intestine**
261
262 Concentrations of measured elements in acanthocephalans followed the order: Ca > Na >
263 Cu > Fe > Tl > Se > Pb, while in intestine of fish host the order was slightly different: Na > Ca >
264 Fe > Cu > Se > Pb >Tl (Table 1). The ratio of metal concentrations in the parasites to those in
265 the fish intestine, called bioconcentration factor (BCF), confirmed more effective metal
266 accumulation of metals in the parasites than in the fish, following the order Tl (69.5)> Ca (34.5)>
267 Cu (23.0)> Pb (12.6)> Fe (1.58)> Se (1.37) = Na (1.37), which mostly confirmed already
268 reported BCF data for the whole population of fish from the Krka River source in spring
269 (Mijošek et al., 2020, Mijošek et al., 2022). This order of BCF values is consistent with literature

data, which also confirmed higher BCFs in different acanthocephalan species than their fish hosts (Sures et al., 1999; Thielen et al., 2004; Filipović Marijić et al., 2013, 2014), again suggesting possible protective role for the host when dealing with enhanced accumulation of non-essential elements. The higher absorption of non-essential elements was explained by the parasites' dependence on host micronutrients, as they lack a gastrointestinal system (Kennedy, 1985). Accordingly, the parasites compete for essential elements from the host intestine, as elements of metabolic importance, but their chemical similarity with toxic metals results in parallel absorption and increased accumulation of non-essential elements (Sures, 2002). Due to such variable concentrations, accumulation pattern and BCFs of metals in acanthocephalans, these trace and macroelements were therefore selected for NanoSIMS analysis to compare their possible variations in metal localisation.

Table 1. Metal concentrations of analysed metals in *Dentitruncus truttae* and intestinal tissue of brown trout specimens from the Krka River (mean ± S.D., n=10)

	Microelements/ µg g^{-1}					**Macroelements/ mg g^{-1}**	
	Cu	**Fe**	**Pb**	**Se**	**Tl**	**Ca**	**Na**
Parasite	15.9±0.4	11.9±0.8	0.63±0.01	0.92±0.06	2.78±0.04	4.48±0.15	1.56±0.79
Intestinal tissue	0.69±0.21	7.54±2.94	0.05±0.01	0.67±0.11	0.04±0.02	0.13±0.06	1.14±0.14

3.2 Ultrastructure of the anterior metasoma of *D. truttae*

The selected acanthocephalan body part, anterior metasoma, is covered by tegument and surrounded by trunk spines, as seen in Fig. 1a. Since hooks (or spines when found on the metasoma) are the most representative structure of acanthocephalans, we selected trunk spine, proboscis retractor (inner part of the parasite body) and inner surface of the tegument (Fig. 1b), as three specific spots for comparison of element localisation in the parasite body. Additionally, the ultrastructure of each of the three selected areas of the anterior portion of trunk of *D. truttae* was for the first time analysed using transmission electron microscopy.

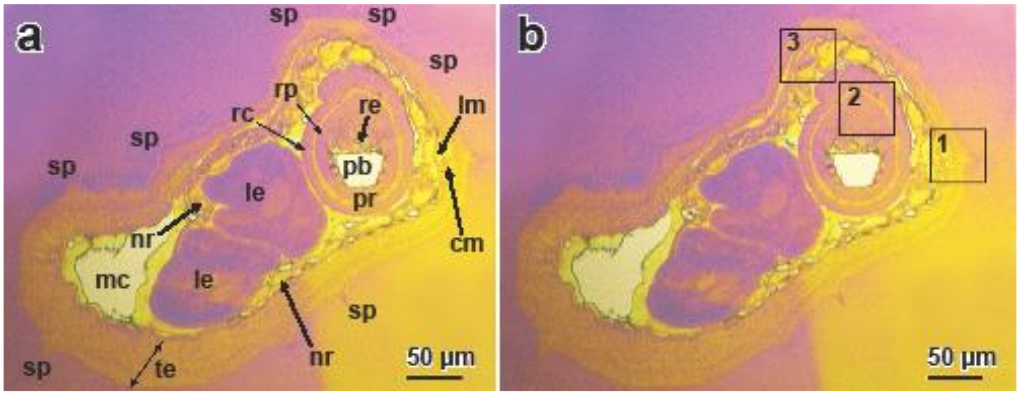

Figure 1. Micrographs of a cross-section of the anterior metasoma of *Dentitruncus truttae* obtained with the optical CCD charge-coupled device (CCD) camera of NanoSIMS. a) Internal and external structures; b) Overview and orientation of the three areas of 50 µm × 50 µm chosen for TEM analysis and element localisation by NanoSIMS: 1 – trunk spine; 2 – proboscis receptacle; 3 –inner surface of the tegument. *Abbreviations:* cm, circular musculature; le, lemniscus; lm; longitudinal musculature; mc, metasoma cavity; nr, neck retractor; pb, body

cavity of the proboscis receptacle; pr, double-walled proboscis receptacle; rc, receptacle constrictor; re, proboscis retractor; rp, receptacle; sp, trunk spine; te, tegument.

3.2.1 Trunk spines

High magnification with TEM micrographs shows three specific layers, i.e., striped, feltwork and radial, in the tegument surrounding the trunk spines of *D. truttae* (Fig. 2a). The striped layer, with an approximate thickness variable from 1.3 to 3.7 μm, is covered by a thin glycocalyx (Fig. 2b, c). Parallel crypts (or channels) immersed in an electron-dense, homogeneous substance, can be distinguished in the striped layer (Fig. 2b, c). These crypts penetrate the outer part of the tegument (glycocalyx) forming numerous pores (Fig. 2c). The TEM micrographs suggest that the crypts of the striped layer may be connected to vesicle-like structures (third layer *sensu* Dezfuli and Sbrenna, 1990) (Fig. 2c), and extend to the outer part of the feltwork layer (Fig. 2b). The feltwork layer cover and support the trunk spines and is composed by a mesh of fibres running in all directions, (Fig. 2a). The spines of *D. truttae* comprise a central core of connective tissue which is surrounding by an exterior layer of electron-dense amorphic matter of 0.7 to 1.7 μm in thickness (Fig. 2a, b). Numerous crypts containing electron-dense amorphic matter are observed in the distal and proximal extremities of the layer of amorphic matter (Figs. 2a, b). The crypts of amorphic matter of the distal extremity are less densely set than those of the proximal extremity (Fig. 2a), but are somewhat thicker, and may reach the posterior part of the striped layer (Fig. 2a, b). Beneath the feltwork layer the radial layer is observed (Fig. 2a).

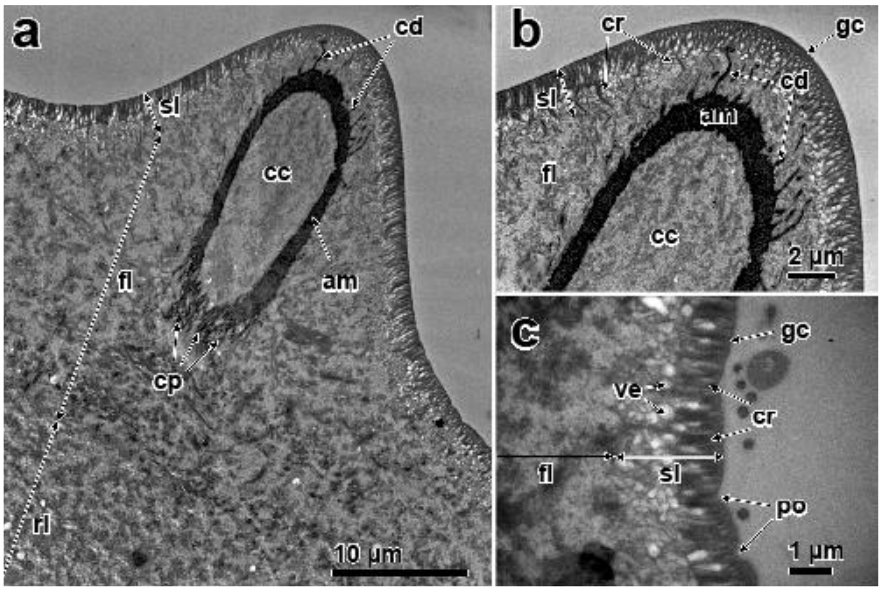

328

329

330 **Figure 2**. Transmission electron micrographs of cross-section of a trunk spine and tegument
331 surface of *Dentitruncus truttae* (see Fig.1b, area 1). a) Trunk spine and surrounding tegument; b)
332 Enlargement of the shaft of a spine and crypts of the layer of amorphic matter; c) Section of
333 tegument surface showing the striped layer above the feltwork layer. *Abbreviations:* am, layer of
334 electron-dense amorphic matter; cc, central core of trunk spine; cd, distal crypts of the layer of
335 amorphic matter; cp, proximal crypts of the layer of amorphic matter; cr, crypts within striped
336 layer; fl, feltwork layer; gc, glycocalyx; po, pore openings; rl, radial layer; sl, striped layer; ve,
337 vesicle-like structures.

338

339 **3.2.2 Proboscis receptacle**

340

341 Similar to other members of the class Palaeacanthocephala, the proboscis receptacle of *D.*
342 *truttae* is double walled. This organ is formed by two muscles, the receptacle constrictor and the
343 receptacle (Fig. 3a, b), which are symmetrically arranged in the proboscis receptable (Fig. 1a).

The receptacle constrictor and the receptacle have somewhat similar organization (Fig. 3a), both comprises of a strong peripherical layer of contractile filaments and a thin cytoplasmic inner lining (Fig. 3a, b); however, the cytoplasmic lining of the receptacle constrictor is divided in two sublayers (Fig. 3b). A layer of extracellular matrix separates the receptacle constrictor from the receptacle. Finally, the proboscis retractor consists of transversally oriented muscle fibres located within the proboscis receptacle (Fig. 3a). These muscles have an asymmetrical arrangement, since they appear confined only to one-half of the inner space or the proboscis receptable (Fig. 1a).

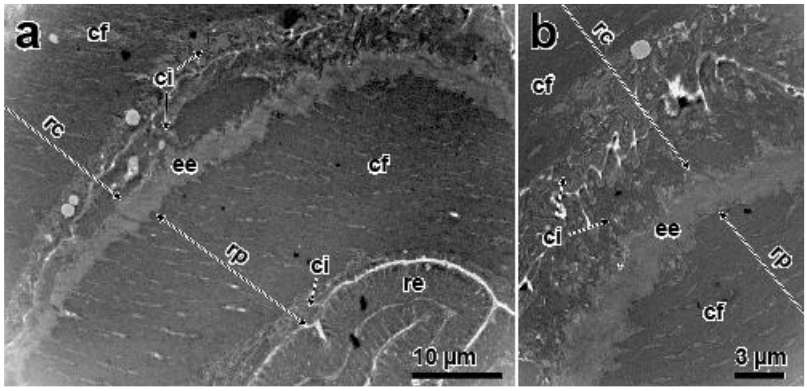

Figure 3. Transmission electron micrographs of cross-section of the proboscis receptacle of *Dentitruncus truttae* (see Fig.1b, area 2). a) Higher magnification of the proboscis receptacle musculature; b) Detail of the cytoplasmic lining and the extracellular matrix between the inner and outer walls of the proboscis receptacle. *Abbreviation:* cf, contractile filaments; ci, cytoplasmic lining; ee, extracellular matrix; rc, receptacle constrictor; re, proboscis retractor; rp, receptacle.

3.2.3 Inner surface of the tegument

The inner surface of the tegument of the anterior metasoma of *D. truttae* is mainly composed by the radial layer, which possess numerous fibres without an apparent definite arrangement (Fig. 4a). A very thin electro-dense basal plate lies beneath the radial layer (Figs. 4a, b). Under the metasoma tegument, an outer coat of circular musculature and an inner coat of longitudinal musculature (Fig. 4b) are observed, both of which are supported by connective tissue. Circular and longitudinal musculature are divided into a peripherical layer of contractile filaments surrounding a central cytoplasm core (Fig. 4a, b), which contained glycogen particles (Fig. 4b). Similar to the musculature beneath the tegument, the neck retractor consists of the contractile layer that surrounds the cytoplasm (Fig. 4a, b). The neck retractor is located in the metasoma cavity, somewhat continuous with the longitudinal musculature (Figs. 1a, 4a).

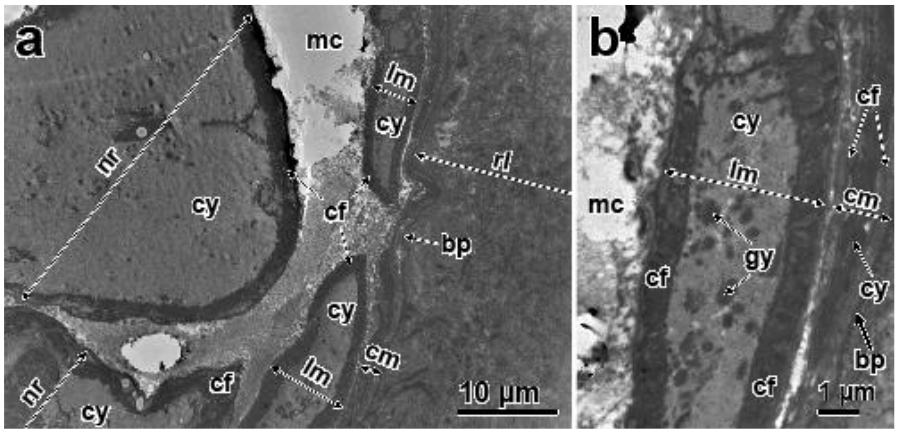

Figure 4. Transmission electron micrographs of cross-section of the inner surface of the tegument of *Dentitruncus truttae* (see Fig.1b, area 3). a) Musculature beneath the tegument; b) Detail of longitudinal and circular musculature. *Abbreviation:* bp, basal plate; cf, contractile

filaments; cm, circular musculature; cy, central cytoplasmic core; gy, glycogen particles; lm, longitudinal muscle; mc, metasoma cavity; nr, neck retractor; rl, radial layer.

3.3 NanoSIMS mapping of chemical elements in the anterior metasoma of *D. truttae* and correlative TEM-NanoSIMS imaging

In contrast to previous studies, which used less sensitive energy dispersive X-ray analysis for low spatially-resolved elemental detection in micrometer-sized spots, our study presents for the first time NanoSIMS data for high-resolution mapping of chemical elements in three acanthocephalan body parts. In addition, NanoSIMS images were correlated to TEM of the same sample areas in order to assign NanoSIMS data to the ultrastructure of *D. truttae*. Moreover, the high sensitivity of NanoSIMS allowed the detection of some trace elements. Analysed chemical elements, ^{12}C, ^{40}Ca, ^{63}Cu, ^{56}Fe, N (as $^{12}C^{14}N^-$), ^{23}Na, ^{16}O, P (as $^{31}P^{16}O_2^-$), ^{208}Pb, ^{32}S, ^{80}Se, and ^{205}Tl showed different localisation regarding specific body structures. The presence of Na, Ca, S, C, N, O was the highest, confirming their importance as essential elements for living cells (Figs. 5, 6, 7). Some non-essential elements, like Tl and Pb, were barely detected by NanoSIMS, indicating their lower content in the analysed structures. This observation was also confirmed by metal levels in tissue, which were the lowest for Tl and Pb in parasites and the intestine of their fish hosts (Table 1). Such results are in accordance to their very low concentration in river water during the same sampling campaign which confirms their low availability for organisms (Dragun et al., 2018; Sertić Perić et al., 2018). Selenium signals appeared in all samples to be within the noise level and did not show clear pattern (data not shown). All samples were firstly analysed by the O^- primary source and afterwards with the Cs^+ source. The analysis of the same area using a

second ion source, after a previous analysis by the opposite source, is known to decrease the sensitivity for the elements of choice. However, this does not hinder the detection of major elements such as C, N, S and P, but it significantly affects microelements like Se, resulting in low Se secondary ion yield and thus low Se visibility. Apart from that, Se concentration in water samples was also low, even below LOD which was <0.059 μg L^{-1} (Dragun et al., 2018). Specific accumulation and localisation of elements in three different areas, namely the trunk spines, tegument and proboscis receptacle of *D. truttae*, are further shown and discussed in Figs. 5, 6 and 7.

3.3.1 Trunk spines

NanoSIMS analyses showed the highest element accumulation in the central part of the trunk spines, involving skeletal fibres and surrounding substances concentrated around them. Carbon is an element found in all biological structures, as reflected by its high presence in all structures, but is also present in the epoxy resin, and so a high signal was detected, too, outside the body (Fig. 5b). Sulfur, Na and Ca were highly concentrated in a circular structure (Fig. 5) corresponding to the amorphic matter identified by TEM, and to a lower extent Fe, while N and P were concentrated in the central core of the trunk spine, but not in the circular structure. Moreover, Ca, N and P were found, too, in high concentration in the whole spine area, confirming the presence of these essential elements characteristic for living cells. Copper was detected in lower concentration, as well as the non-essential metal, Tl, which was detected in a very low concentration, distributed homogeneously in the body. Trunk spines represent the only area of acanthocephalans where we could observe some Tl signal. The presence of Pb was

negligible in this area, although some previous preliminary studies indicated the presence of Pb in the hooks of acanthocephalans (as mentioned by Sures et al., 1999). However, concentrations of these non-essential metals were low in the investigated acanthocephalan species from the Krka River (Fig. 5).

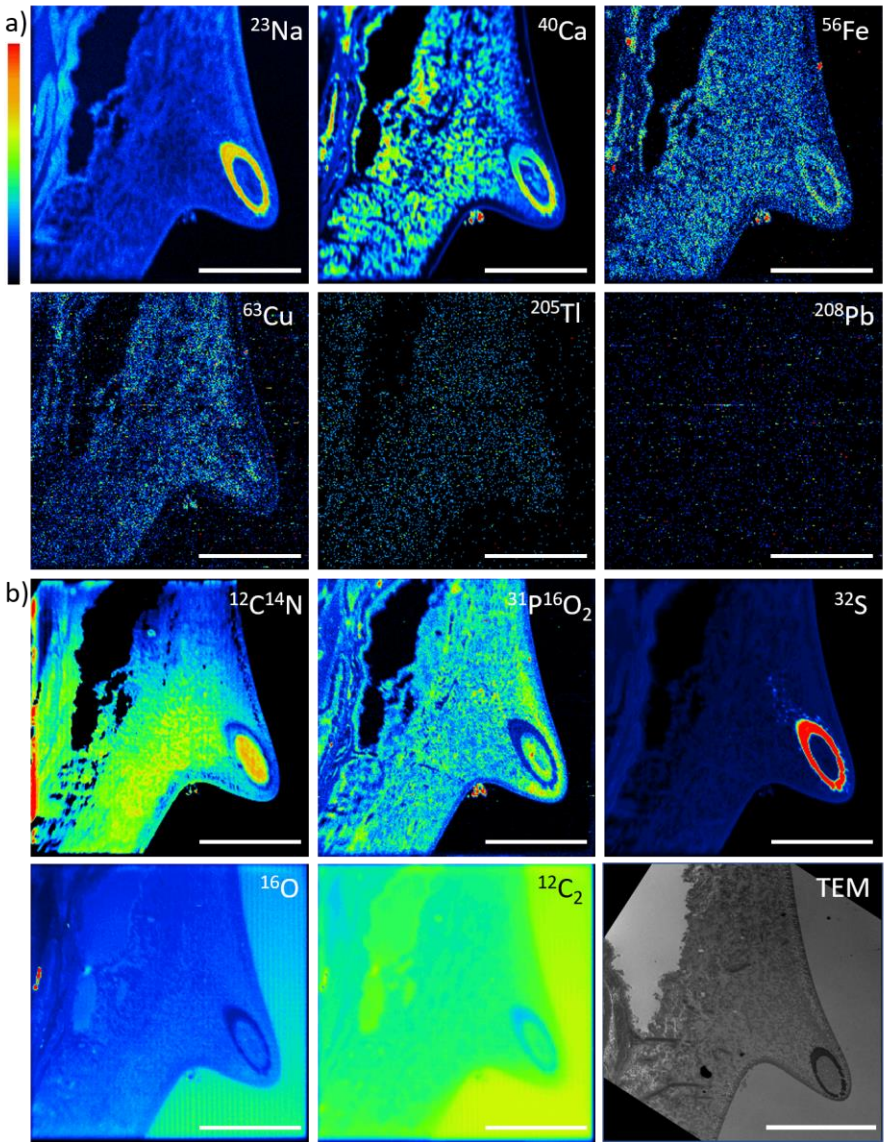

Figure 5. Elemental mapping of the trunk spines (see Fig.1b, area 1) of *Dentitruncus truttae* by NanoSIMS using: a) O^- source: $^{23}Na^+$, $^{40}Ca^+$, $^{56}Fe^+$, $^{63}Cu^+$, $^{205}Tl^+$, $^{208}Pb^+$; b) Cs^+ source: $^{12}C^{14}N^-$, $^{31}PO_2^-$, $^{32}S^-$, $^{16}O^-$, $^{12}C^2$, as well as correlative imaging with TEM of the same sample area from a

435 subsequent ultramicrotome section. Color scale on the top left represents relative intensities of
436 the isotopes count rates. Scale bar: 20 µm.
437
438 Our data are in accordance with previous studies using X-ray spot analyses such as Brázová
439 et al. (2014) who found Ca as the dominant element in all parts of the proboscis hooks of another
440 spiny-headed worm with aquatic life cycle, *Acanthocephalus lucii* (Müller, 1776), followed by S
441 and P. The authors explained the high presence of Ca and P by forming a rigid calcium
442 phosphate apatite with disulfide bonds (thiol groups of the amino acids cysteine and cystine),
443 which represents the hardest tissue found in invertebrates (Luz and Mano, 2010). Moreover, the
444 lower content of S, Ca and P in the proximal region of the hook of *A. lucii* was explained by
445 providing flexibility to hooks, while presence of S in the outermost layer of the hook enhances
446 its hardness and attachment to the epithelium of the host's intestine (Brázová et al., 2014). A
447 similar observation was reported by Heckmann et al. (2012b) who localised Ca and P in basal
448 hooks and S in apical part of the hooks, and reported element order S > Ca > P in the proboscis
449 hooks of *Rhadinorhynchus ornatus* Van Cleave, 1918 using Energy Dispersive X-Ray Analysis
450 (EDXA). High concentrations of S at proboscis and hooks of five acanthocephalans, namely
451 *Neoechinorhynchus qatarensis* (Amin et al., 2002); *Acanthocephalus dirus* Van Cleave, 1931,
452 *Neoechinorhynchus idahoensis* (Amin and Heckmann, 1992), *Echinorhynchus salmonis* Müller,
453 1784, and *Pseudoacanthocephalus* sp., were also reported by Heckmann et al. (2007). Our data
454 for *D. truttae* provide a first high-resolution insight to the distribution of chemical elements.
455 Owing to TEM-NanoSIMS correlative imaging, the high S, Na and Ca concentrations in hooks
456 described in previous studies can now be unambiguously assigned to a circular structure of
457 amorphic matter that contains also the trace metal Fe. In contrast, this circular amorphic matter

458 lacks of P, thus the high-resolved element map revealed that Ca and P are not co-localised in this
459 structure, which contests the possible formation of calcium phosphate apatite hypothesized by
460 Brázová et al. (2014).
461
462 **3.3.2 Proboscis receptacle**
463
464 Till now, only the morphology but not the element distribution of the proboscis was only
465 studied using light, transmission and scanning electron microscopy (Taraschewski, 2000).
466 NanoSIMS imaging provided insight into the distribution of chemical elements in the
467 ultrastructure of the proboscis receptacle of *D. truttae* (Fig. 6.). The most dominant element in
468 the proboscis receptacle was Ca, mostly located in the cytoplasmic inner lining and the proboscis
469 retractor muscles, but its presence could be observed in other parts as well. Similarly, Na, Fe, Cu,
470 S, N and P occurred mostly in the proboscis retractor muscle, but these elements varied in their
471 intensities and distribution (Fig. 6). Further, Fe and Cu showed an overlay with O in few
472 hotspots, possible indicating the presence of metallic oxides deposits. As in trunk spine, Tl, Pb
473 and Se (not shown) mapping did not show any pattern (Fig. 6).
474

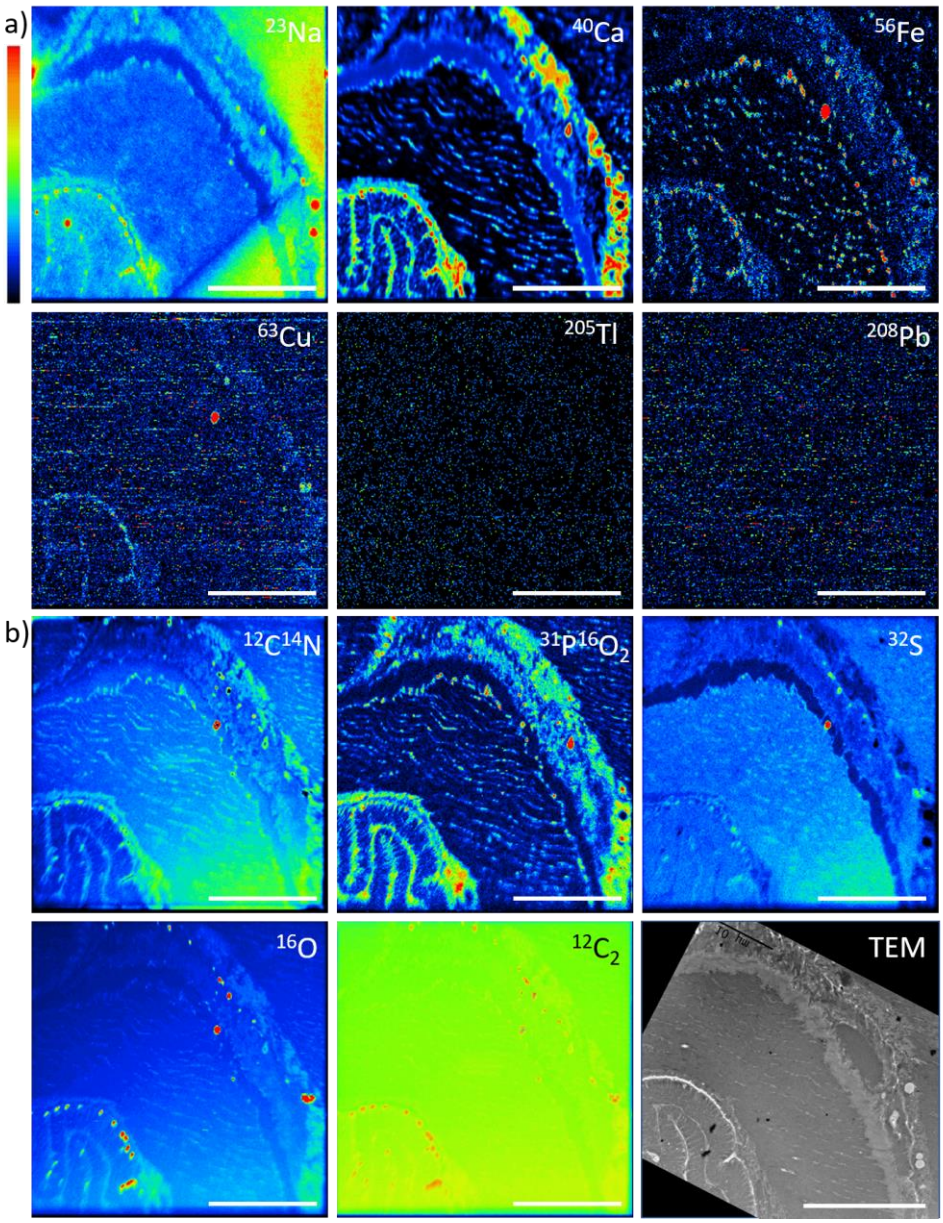

475

476

477 **Figure 6**. Elemental mapping of the proboscis receptacle (see Fig.1b, area 2) of *Dentitruncus*

478 *truttae* by NanoSIMS using: a) O^- source: $^{23}Na^+$, $^{40}Ca^+$, $^{56}Fe^+$, $^{63}Cu^+$, $^{205}Tl^+$, $^{208}Pb^+$; b) Cs^+ source:

479 $^{12}C^{14}N^-$, $^{31}PO_2^-$, $^{32}S^-$, $^{16}O^-$, $^{12}C^2$, as well as correlative imaging with TEM of the same sample area

480 from a subsequent ultramicrotome section. Color scale on the top left represents relative

intensities of the isotopes count rates. Scale bar: 20 µm. Colour scale corresponds to relative concentration of elements.

3.3.3 Inner surface of the tegument

In addition, NanoSIMS provided first data on elemental distribution in the ultrastructure of the tegument of *D. truttae* (Fig. 7). The superficial layer of the acanthocephalan tegument also had a higher concentration of S, Na and Ca than the circular and longitudinal musculature. Sulfur and Na were mostly localised in contractile filaments of the muscle, while Ca was found mostly in the central cytoplasmic core of longitudinal muscles and the neck retractor muscles (Fig. 7). Sodium was also partially present in the same areas, showing few hotspots in the neck retractor area (Fig. 7). Among other measured elements, only Fe and P were observed in the circular and longitudinal musculature. Similar to the trunk spines (outer tegument), Fe and Cu were predominant metals in the acanthocephalan inner tegument, whereas Se (not shown), Tl and Pb were not detected in this part either (Fig. 7).

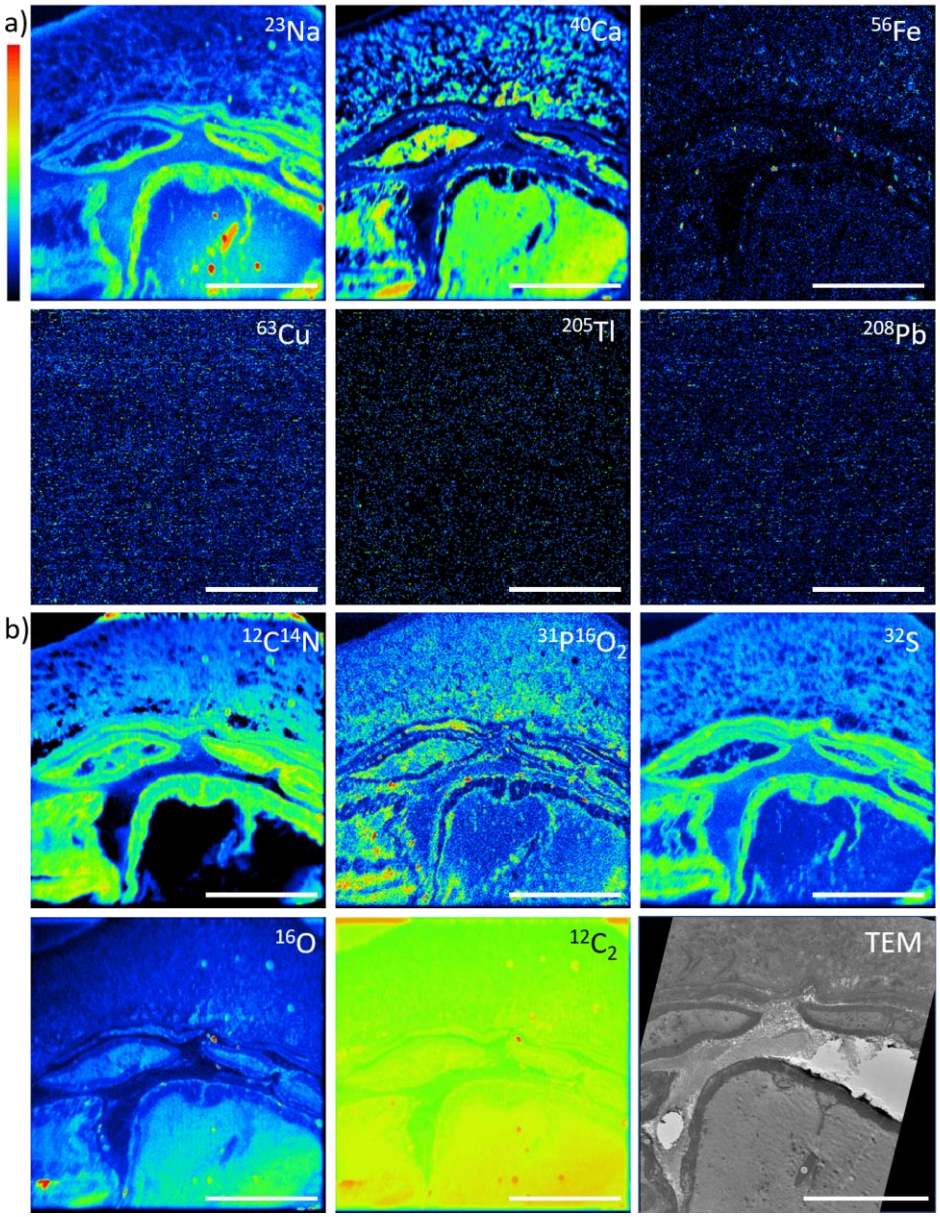

497

498

499 **Figure 7.** Elemental mapping of the tegument (see Fig.1b, area 3) of *Dentitruncus truttae* by

500 NanoSIMS using: a) O^- source: $^{23}Na^+$, $^{40}Ca^+$, $^{56}Fe^+$, $^{63}Cu^+$, $^{205}Tl^+$, $^{208}Pb^+$; b) Cs^+ source: $^{12}C^{14}N^-$,

501 $^{31}PO_2^-$, $^{32}S^-$, $^{16}O^-$, $^{12}C^2$, as well as correlative imaging with TEM of the same sample area from a

502 subsequent ultramicrotome section. Color scale on the top left represents relative intensities of

503 the isotopes count rates. Scale bar: 20 µm. Colour scale corresponds to relative concentration of
504 elements.
505
506 **4. CONCLUSIONS**
507
508 Our results represent important initial data with a perspective for the use of NanoSIMS in
509 parasitology and environmental studies in general, in spite of few limitations of our study with
510 respect to the methodology and low environmental metal concentrations. The first description of
511 the chemical composition of the acanthocephalan body at nanometer level indicates complex
512 structures that varies in element localisation. It was furthermore possible to link the distribution
513 of chemical elements to the acanthocephalan ultrastructure to TEM-NanoSIMS correlative
514 imaging. The highest concentration in all studied structures was confirmed for Na, Ca, S, C, N,
515 O, as essential and constitutive elements in living cells. The high amount of S found in trunk
516 spines could be explained for the first time by linking its presence to a circular structure of
517 amorphic matter. A high amount of Na was localised, too, in this circular structure of the spines,
518 and as well in contractile filaments of the muscles. Calcium was dominantly found in the
519 cytoplasmic inner lining and the proboscis retractor muscles and as well in the spine circular
520 structure. As for trace metals, Fe was predominant in all studied structures, while Cu showed the
521 same pattern in the proboscis receptacle and trunk spines, but no concentration in the tegument.
522 Lead and Tl concentrations were generally low in the environment and the parasite so its
523 detection by NanoSIMS was not efficient, but we could still observe some shapes of Tl
524 localisation in the region of the trunk spines compared with other two areas. Generally, non-

essential metals were mostly distributed in small concentrations along investigated structures and did not show distinctive locations for accumulation in the parasite's body.

High-resolution localisation of chemical elements by NanoSIMS confirmed the highest density of essential elements characteristic for living cells and their specific incorporation in different body parts of the acanthocephalan *D. truttae*. Trunk spines and tegument showed mostly higher element accumulation than the proboscis receptacle, probably reflecting their role in substance absorbance in the organisms. Further analyses on element localisation are needed to compare element distribution in parasites found in hosts exposed to different environmental conditions, such as unpolluted and pollution-impacted sites, as well as to compare NanoSIMS data between different acanthocephalan species.

Funding Sources

The research was supported by the Croatian Science Foundation within the project no. IP-2014-09-4255 "Accumulation, Subcellular Mapping and Effects of Trace Metals in Aquatic Organisms" (AQUAMAPMET).

Acknowledgements

The authors acknowledge the Czech Science Foundation (project No. 19-28399X) and the Czech Academy of Sciences (RVO: 60077344) and are sincerely grateful for the help in TEM electronic imaging to the Bordeaux Imaging Center (member of the France BioImaging national infrastructure, ANR-10-INBS-04) and for the fieldwork assistance to the members of the

Laboratory for Biological Effects of Metals and Laboratory for Aquaculture and Pathology of Aquatic Organisms (Ruđer Bošković Institute, Croatia).

REFERENCES

Amin, O. M., Heckmann, R. A. 1992. Description and Pathology of *Neoechinorhynchus idahoensis* n. sp. (Acanthocephala: Neoechinorhynchidae) in *Catostomus columbianus* from Idaho. J. Parasitol. 78(1), 34-39. https://doi.org/10.2307/3283682.

Amin, O. M., Saoud, M. F. A., Alkuwari, K. S. R., 2002. *Neoechinorhynchus qatarensis* sp. n. (Acanthocephala: Neoechinorhynchidae) from the blue-barred flame parrot fish, *Scarus ghobban* Forsskål, 1775, in Qatari waters of the Arabian Gulf. Parasitol. Int. 51(2), 171-176. doi: 10.1016/s1383-5769(02)00011-9.

Beermann I., Arai H. P., Costerton J. W.,1974. The ultrastructure of the leminisci and body wall of *Octospinifer macilentus* (Acanthocephala). Can. J. Zool. *52*, 553–555.

Brázová, T., Poddubnaya, L. G., Ramírez Miss, N., Hanzelová, V., 2014. Ultrastructure and chemical composition of the proboscis hooks of *Acanthocephalus lucii* (Müller, 1776) (Acanthocephala: Palaeacanthocephala) using X-ray elemental analysis. Folia Parasit. 61, 549–557.

Dezfuli, B., Sbrenna, G., 1990. A morphological and ultrastructural study of *Telosentis exiguus* (Acanthocephala, Palaeacanthocephala). Ital. J. Zool. 57, 225–232.

570 Dezfuli, B. S., Giovinazzo, G., Lui, A., Giari, L., 2008a. Inflammatory response to *Dentitruncus*
571 *truttae* (Acanthocephala) in the intestine of brown trout. Fish. Shellfish. Immun. 24, 726–733.
572 Dezfuli, B. S., Lui, A., Giari, L., Boldrini, P., Giovinazzo, G., 2008b. Ultrastructural study on the
573 body surface of the acanthocephalan parasite *Dentitruncus truttae* in brown trout. Microsc.
574 Res. Techniq. 71, 230–235.
575 Filipović Marijić, V., Vardić Smrzlić, I., Raspor, B., 2013. Effect of acanthocephalan infection
576 on metal, total protein and metallothionein concentrations in European chub from a Sava
577 River section with low metal contamination. Sci. Total Environ. 463/464, 772–780.
578 Filipović Marijić, V., Vardić Smrzlić, I., Raspor, B., 2014. Does fish reproduction and metabolic
579 activity influence metal levels in fish intestinal parasites, acanthocephalans, during fish
580 spawning and post-spawning period? Chemosphere 112, 449–455.
581 Filipović Marijić, V., Kapetanović, D., Dragun, Z., Valić, D., Krasnići, N., Redžović, Z., Grgić,
582 I., Žunić, J., Kružlicová, D., Nemeček, P., Ivanković, D., Vardić Smrzlić, I., Erk, M., 2018.
583 Influence of technological and municipal wastewaters on vulnerable karst riverine system,
584 Krka River in Croatia. Environ. Sci. Pollut. R. 25, 4715–4727.
585 Filipović Marijić, V., Mijošek, T., Dragun Z., Retzmann A., Zitek A., Prohaska, T., Bačić, N.,
586 Redžović, Z., Grgić, I. Krasnići, N., Valić, D., Kapetanović, D., Žunić, J., Ivanković, D.,
587 Vardić Smrzlić, I., Erk, M., 2022. Application of Calcified Structures in Fish as Indicators of
588 Metal Exposure in Freshwater Ecosystems. Environments 9, 14.
589 https://doi.org/10.3390/environments9020014.
590 Graham, L., Orenstein, J.M., 2007. Processing tissue and cells for transmission electron
591 microscopy in diagnostic pathology and research. Nat. Protoc. 2 (10), 2439-2450.

592 Guerquin-Kern, J-L., Wu, T-D., Quintana, C., Croisy, A., 2005. Progress in analytical imaging of
593 the cell by dynamic secondary ion mass spectrometry (SIMS microscopy). Biochim. Biophys.
594 Acta - General Subjects 1724 (3), 228-238. https://doi.org/10.1016/j.bbagen.2005.05.013.
595 Hayat, M., 1982. Fixation for Electron Microscopy. New York, Academic Press.
596 Heckmann, R. A., Amin, O. M.; Standing, M. D., 2007. Chemical analysis of metals in
597 acanthocephalans using Energy Dispersive XRay Analysis (EDXA) in conjunction with a
598 Scanning Electron Microscope (SEM). Comp. Parasitol. 74, 388–391.
599 https://doi.org/10.1654/4258.1.
600 Heckmann, R. A., Amin, O. M., Radwan, N. A. E., Standing, M. D., Eggett, D. L., 2012a.
601 Comparative chemical element analysis using Energy Dispersive Xray Microanalysis
602 (EDXA) for four species of Acanthocephala. Sci. Parasitol. 13, 27–35.
603 Heckmann, R. A., Amin, O. M., Radwan, N. A., Standing, M. D., Eggett, D. L., El Naggar, A.
604 M., 2012b. Fine structure and Energy Dispersive X-Ray Analysis (EDXA) of the proboscis
605 hooks of *Rhadinorhynchus ornatus*, Van Cleave 1918 (Rhadinorhynchidae: Acanthocephala).
606 Sci. Parasitol. 13, 37–43.
607 Herlyn, H., Ehlers U., 2001. Organisation of the praesoma in *Acanthocephalus anguillae*
608 (Acanthocephala, Palaeacanthocephala) with special reference to the muscular system.
609 Zoomorphology 121, 13–18.
610 Herlyn, H., Taraschewski, H., 2017. Evolutionary anatomy of the muscular apparatus involved in
611 the anchoring of Acanthocephala to the intestinal wall of their vertebrate hosts. Parasitol. Res.
612 116, 1207–1225.
613 HRN EN 14011, Fish sampling by electric power (In Croatian). Croatian Standard Institute,
614 Zagreb (2005).

615 Kennedy, C.R., 1985. Regulation and dynamics of acanthocephalan population. In Biology of the
616 Acanthocephala, Crompton, D. W. T., Nickol B. B. (Eds.), Cambridge University Press:
617 Cambridge; pp. 385–416.
618 Kennedy C.R., 2006. Ecology of the Acanthocephala, Cambridge University Press, Cambridge.
619 Kleinfeld, A. M., Kampf, J. P., Lechene, C., 2004. Transport of 13C-oleate in adipocytes
620 measured using multi imaging mass spectrometry. J. Am. Soc. Mass Spectr. 15, 1572–1580.
621 Luz, G. M., Mano, J. F., 2010. Mineralized structures in Nature: examples and inspirations for
622 the design of new composite materials and biomaterials. Compos. Sci. Technol. 70, 1777-
623 1788.
624 Malherbe, J., Penen, F., Isaure, M-P., Frank, J., Hause, G., Dobritzsch, D., Gontier, E., Horréard,
625 F., Hillion, F., Schaumlöffel, D., 2016. A new radio frequency plasma oxygen primary ion
626 source on nano secondary ion mass spectrometry for improved lateral resolution and detection
627 of electropositive elements at single cell level. Anal. Chem. 88, 7130–7136. https://doi.org/
628 10.1021/acs.analchem.6b01153.
629 Manilla, G., Orecchia, P., Paggi, L., 1976. Parassitofauna di *Salmo trutta* L. del fiume Tirino.
630 Nota I. Ridescrizione di *Dentitruncus truttae* Sinzar, 1955 e considerazioni sul genere
631 Dentitruncus Sinzar, 1955. Parassitologia 18, 71–78.
632 Mauer, K. M., Schmidt, H., Dittrich, M., Fröbius, A. C., Hellmann, S. L., Zischler, H., Hankeln,
633 T., Herlyn, H., 2021. Genomics and transcriptomics of epizoic Seisonidea (Rotifera, syn.
634 Syndermata) reveal strain formation and gradual gene loss with growing ties to the host. BMC
635 Genomics 22: 604.
636 Mijošek, T., Filipović Marijić, V., Dragun, Z., Ivanković, D., Krasnići, N., Redžović, Z., Veseli,
637 M., Gottstein, S., Lajtner, J., Sertić Perić, M., Matoničkin Kepčija, R., Erk, M., 2020.

638 Thallium accumulation in different organisms from karst and lowland rivers of Croatia under
639 wastewater impact. Environ. Chem. 17 (2), 201-212
640 Mijošek, T., Filipović Marijić, V., Dragun, Z., Ivanković, D., Krasnići, N., Erk, M., 2022.
641 Efficiency of metal bioaccumulation in acanthocephalans, gammarids and fish in relation to
642 metal exposure conditions in a karst freshwater ecosystem. J. Trace Elem. Med. Bio. 73,
643 127037. https://doi.org/ 10.1016/j.jtemb.2022.127037.
644 Nachev, M., Schertzinger, G., Sures, B., 2013. Comparison of the metal accumulation capacity
645 between the acanthocephalan *Pomphorhynchus laevis* and larval nematodes of the genus
646 *Eustrongylides* sp. infecting barbel (*Barbus barbus*). Parasite Vector. 6,
647 https://doi.org/10.1186/1756-3305-6-21.
648 Oyoo-Okoth, E., Admiraal, W., Osano, O., Kraak, M.H.S., Gichuki, J., Ogwai, C., 2012.
649 Parasites modify sub-cellular partitioning of metals in the gut of fish. Aquat. Toxicol. 106–
650 107, 76–84.
651 Schroeder, J.A., Gelderblom, H.R., Hauroeder, B., Schmetz, C., Milios, J., Hofstaedter, F., 2006.
652 Microwave-assisted tissue processing for same-day EM-diagnosis of potential bioterrorism
653 and clinical samples. Micron 37 (6), 577-590, https://doi.org/10.1016/j.micron.2005.11.015
654
655 Sertić Perić, M., Matoničkin Kepčija, R., Miliša, M., Gottstein, S., Lajtner, J., Dragun, Z.,
656 Filipović Marijić, V., Krasnići, N., Ivanković, D., Erk, M., 2018. Benthos-drift relationships
657 as proxies for the detection of the most suitable bioindicator taxa in flowing waters – a pilot-
658 study within a Mediterranean karst river. Ecotox. Environ. Safe. 163, 125–135.
659
660

661 Sures, B., 2002. Competition for minerals between *Acanthocephalus lucii* and its definitive host
662 perch (*Perca fluviatilis*). Int. J. Parasitol. *32*, 1117–1122.
663 Sures, B., 2004. Environmental parasitology: relevancy of parasites in monitoring environmental
664 pollution. Trends. Parasitol. 20, 170-177.
665 Sures, B., Siddall, R., 2003. Uptake and accumulation of lead by the parasitic worm
666 *Pomphorhynchus laevis* (Palaeacanthocephala) in the intestine of chub (*Leuciscus cephalus*).
667 Int. J. Parasitol. 33, 65–70.
668 Sures, B., Siddall, R., Taraschewski, H., 1999. Parasites as accumulation indicators of heavy
669 metal pollution. Parasitol. Today 15, 16–21.
670 Šinžar, D., 1955. Prilog poznavanju endoparazita pastrmke *Salmo trutta* L. (In Serbian) [A
671 contribution to the knowledge of endoparasites of trout *Salmo trutta* L.]. Glasnik Prirod.
672 Muzeja Srp. Zemlje B 7, 4.
673 Taraschewski, H., 2000. Host-parasite interactions in Acanthocephala: a morphological
674 approach. Adv. Parasit. 46, 1–179.
675 Thielen, F., Zimmermann, S., Baska, F., Taraschewski, H., Sures, B., 2004. The intestinal
676 parasite *Pomphorhynchus laevis* (Acanthocephala) from barbel as a bioindicator for metal
677 pollution in the Danube River near Budapest, Hungary. Environ. Pollut. 129, 421–429.
678 Topić Popović, N., Strunjak-Perović, I., Fonns, A., Vilsgaard-Espersen, T., Teskeredžić, E.,
679 1999. *Pseudorhadinorhynchus salmothymi* isolation from brown trout in Krka river (Croatia).
680 Period. Biol. 101, 273–275.
681 Vardić Smrzlić, I., Valić, D., Kapetanović, D., Dragun, Z., Gjurčević, E., Ćetković, H.,
682 Teskeredžić, E., 2013. Molecular characterisation and infection dynamics of *Dentitruncus*

683 *truttae* from trout (*Salmo trutta* and *Oncorhynchus mykiss*) in Krka River, Croatia. Vet.
684 Parasitol. 197, 604–613.
685
686
687
688